Biosensors and Bioelectronics 138 (2019) 111319

Contents lists available at ScienceDirect

Biosensors and Bioelectronics

journal homepage: www.elsevier.com/locate/bios

A versatile dynamic light scattering strategy for the sensitive detection of microRNAs based on plasmonic core – satellites nanoassembly coupled with strand displacement reaction

Ganglin Wang[a], Mingxia Yu[b], Guoping Wang[a,*]

[a] Hubei Bioinformatics & Molecular Imaging Key Laboratory, Department of Biomedical Engineering, College of Life Science and Technology, Huazhong University of Science and Technology, Wuhan, 430074, Hubei, PR China
[b] Department of Clinical Laboratory, Zhongnan Hospital of Wuhan University, Wuhan, Hubei, 430071, PR China

ARTICLE INFO

Keywords:
Gold nanoparticle
Dynamic light scattering
microRNA
Strand displacement reaction
Core-satellites nanoassembly

ABSTRACT

A low-cost, effective and enzyme-free sensing strategy for ultrasensitive microRNA (miRNA) detection was developed based on dynamic light scattering (DLS) coupled with strand displacement reaction (SDR). The combination of DLS and SDR was used to assess the size changes of core-satellites nanoassembly. This strategy realized the limit of detection (LOD) as low as 0.24 pM (S/N = 3) and the detection range of 5 pM–150 pM, which might urge this strategy as an ideal candidate for the sensitive detection of miRNA in the future. In addition, the proposed strategy could be successfully used to analyze target miRNA in various cancer cells, indicating that the developed SDR-DLS strategy has promising clinical implications for rapid and early diagnosis of cancer-related diseases.

1. Introduction

MicroRNAs (miRNAs) are endogenous non-coding small RNAs of approximately 21–24 nucleotides that involve in the regulation of gene expression, and thus play pivotal roles in cell proliferation, differentiation, and apoptosis (Dong et al., 2013; Jonas and Izaurralde, 2015). Previous studies have demonstrated the aberrant miRNA expression levels are closely related to human diseases, including cancers (Boon et al., 2013; Jalava et al., 2012). Hence, monitoring miRNA dysregulation is considered to be a valuable prospect for the identification of cancerous cells and prediction of diseases.

At present, reverse transcription polymerase chain reaction (RT-PCR) (Benes and Castoldi, 2010) and northern blot (Lagos et al., 2001) are the most common approaches for the quantification of miRNAs. However, these methods require sophisticated instruments and labor-intensive procedures (Ma et al., 2017). More importantly, the PCR-based methods have potential to generate false-positive results (Ladetto et al., 2014). Alternatively, a series of new strategies for miRNAs detection based on fluorescence (Yin et al., 2017; Tu et al., 2012), electrochemistry (Yu et al., 2014; Lautner and Gyurcsányi, 2014), colorimetry (Shen et al., 2013; Wu et al., 2016), chemiluminescence (Wang et al., 2016; S. Li et al., 2017), molecular beacons (Bose et al., 2013; Lee et al., 2016) and surface-enhanced Raman scattering (SERS) (Guven et al., 2014; Song et al., 2016) have been proposed in the literature. Each of these strategies possesses its own advantages and disadvantages. For instance, it may be relatively difficult to distinguish minor changes in high-frequency color by naked eyes; fluorescence-labeled probes are prone to rapid photobleaching and the signal intensity may be insufficient for certain applications; SERS and electrochemical methods are rarely used in the recognition of micro-signals, due to low repeatability (Lai et al., 2017, 2018; Qin et al., 2017). Therefore, it is highly desirable to develop simple, inexpensive, rapid, accurate and sensitive methods for the quantitative detection of miRNAs.

Since Mirkin group initially fabricated DNA-functionalized gold nanoparticle (AuNPs), AuNPs-conjugated DNA probes have been proposed for nucleic acid sensing due to their ultrafine size, distance-dependent optical properties and excellent biocompatibility (Elghanian et al., 1997; Lee et al., 2014; Degliangeli et al., 2014; Qin et al., 2018). DNA-modified AuNPs probes are widely applied to fluorescence energy resonance transfer (Zhong et al., 2017), electrochemical (Liu et al., 2015), SERS (He et al., 2019), DLS (Lu et al., 2019) and colorimetric detection of miRNAs (X. Li et al., 2017). However, the sensitivities of these methods were far from satisfactory for measuring the low abundance of miRNAs in real biological samples. Thus, there is an urgent need to develop a novel, simple and reliable AuNPs-based sensing

* Corresponding author.
E-mail address: wangguoping@hust.edu.cn (G. Wang).

https://doi.org/10.1016/j.bios.2019.111319
Received 16 March 2019; Received in revised form 8 May 2019; Accepted 10 May 2019
Available online 13 May 2019
0956-5663/

method with greatly improved sensitivity towards the quantification of low-abundance miRNAs. To overcome the deficiency, signal amplification strategies have gained increasing attention for highly sensitive detection of miRNAs, including rolling circle amplification (RCA) (Xu et al., 2012), enzyme-assisted amplification (Dong et al., 2015), hybridization chain reaction (HCR) (Wu et al., 2015) and toehold-mediated DNA SDR (Liang et al., 2017). Among these techniques, SDR has received considerable attention due to its intrinsic merits, such as isothermal and enzyme-free nature, low cost, protocol simplicity and high amplification efficiency. Thenceforth, the combination of AuNPs and SDR may hold great promise for sensitivity improvement.

Here, we developed a versatile plasmonic core－satellites nanoassembly-based probe for miRNA sensing by combining SDR and DLS as a powerful signal transduction process to monitor AuNPs-mediated cross-linking. To the best of our knowledge, this is the first study to integrate plasmonic nanoparticles with SDR for the highly sensitive detection of miRNA-21. A core－satellites nanoassembly was constructed using the bottom-up strategy. The probe consisted of a core AuNP (C–AuNP) and several satellite AuNPs. (S-AuNPs). S-AuNPs were tethered to C-AuNPs surface via a DNA linker (L), resulting in the formation of core－satellites nanoassembly. The presence of miRNA-21 and fuel DNA strand (fuel) triggered disassembly of the core－satellites nanoassembly probe via the toehold-mediated SDR, leading to the removal of satellite nanoparticles from core nanoparticles. The disassembly of AuNPs core－satellites probes might lead to significant changes in hydrodynamic diameter. With addition of the fuel, the reaction initiated another cycle of reactions catalyzed by miRNA-21 repeatedly, thus the strategy would yield a significantly amplified and higher sensitivity signal. The target-induced size changes of core－satellites nanoassembly probes could be facilely and directly monitored with DLS technique, which was suitable for low abundance biomolecules detections.

2. Results and discussion

The working principle of the proposed SDR-DLS strategy was illustrated in Fig. 1 and Fig. S1. Brifely, the core-satellites nanoassembly was constructed by conjuncting multiple 13 nm satellite-AuNPs onto a 50 nm core-AuNP through the L. Fuel was used to run the DNA circuit. Upon the addition of target miRNA and fuel, the target miRNA directly bounded to the corresponding toehold 1 sequence of the L, which triggered a branch migration reaction, resulting in the displacement of the 13 nm S-AuNPs. As a result, the toehold 2 sequence of the L was exposed and subsequently hybridized with fuel, leading to the dissociation of target miRNA from L. Then, the released target miRNA further hybridized with another toehold 1, and a set of reactions described above were recycled, resulting in the disassembly of the core-satellites nanoassembly and a dramatic decrease in particle size, which can be measured by DLS.

The as-prepared C-AuNPs and S-AuNPs were characterized by transmission electron microscopy (TEM) and UV–vis spectroscopy. The absorption peaks of C-AuNPs and S-AuNPs were located at 532 and 522 nm (Fig. S2), corresponding to the diameters of 50 and 13 nm, respectively. Subsequently, both C-AuNPs and S-AuNPs were co-assembled on the L via DNA hybridization. Assembly of C-AuNPs and S-AuNPs could result in the formation of core-satellites nanostructures, as revealed by agarose gel electrophoresis result (Fig. 2a) and TEM images (Fig. 2b and c). A clear band of C–AuNP was observed in the gel indicating its good dispersity. C–AuNP + L presented a band with a slower migration rate than C–AuNP. After assembly of C-AuNPs and S-AuNPs, the migration rate of the band further decreased, thus representing the successful assembly of core-satellites. There are 10 S-AuNPs on each C–AuNP on average, as calculated from TEM images. More experimental details were provided in Supporting Information. The assembly of core-satellites nanoassembly was further investigated using UV–vis spectroscopy and DLS (Fig. S3). The absorption peak of core-satellites nanoassembly had a redshift to 540 nm, which attributed to the surface plasmon coupling effect between C–AuNP and S-AuNPs. The hydrodynamic sizes of the particles increased to 204.6 nm after the formation of core-satellites nanoassembly. Notably, the core-satellites nanoassemblies are colloidal and stable under different ionic strengths (0–500 mM NaCl) and pH (4.0–10.0), and remain apparently intact in the presence of DNase I (Figs. S5–S7).

To evaluate the feasibility of this strategy, miRNA-21 was selected as a proof-of-concept target. Non-denaturing polyacrylamide gel electrophoresis (PAGE) and agarose gel electrophoresis were carried out to monitor the catalytic reaction. As shown in Fig. 2d and Fig. S4, disassembly of AuNPs with L occurred in the presence of fuel and subtle amount of miRNA-21 catalyst, resulting in the new band of S-AuNPs in the gel. (lane 7 and 8) Upon comparison, no changes were observed in

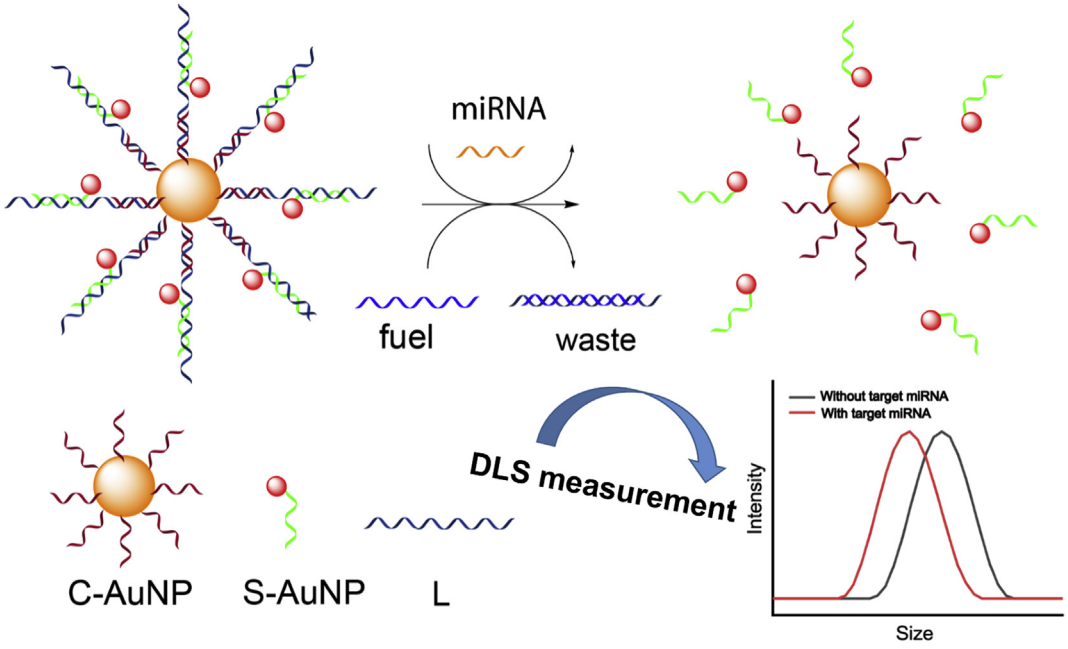

Fig. 1. Schematic illustration of plasmonic core-satellites structures coupled with toehold-mediated DNA strand displacement reaction.

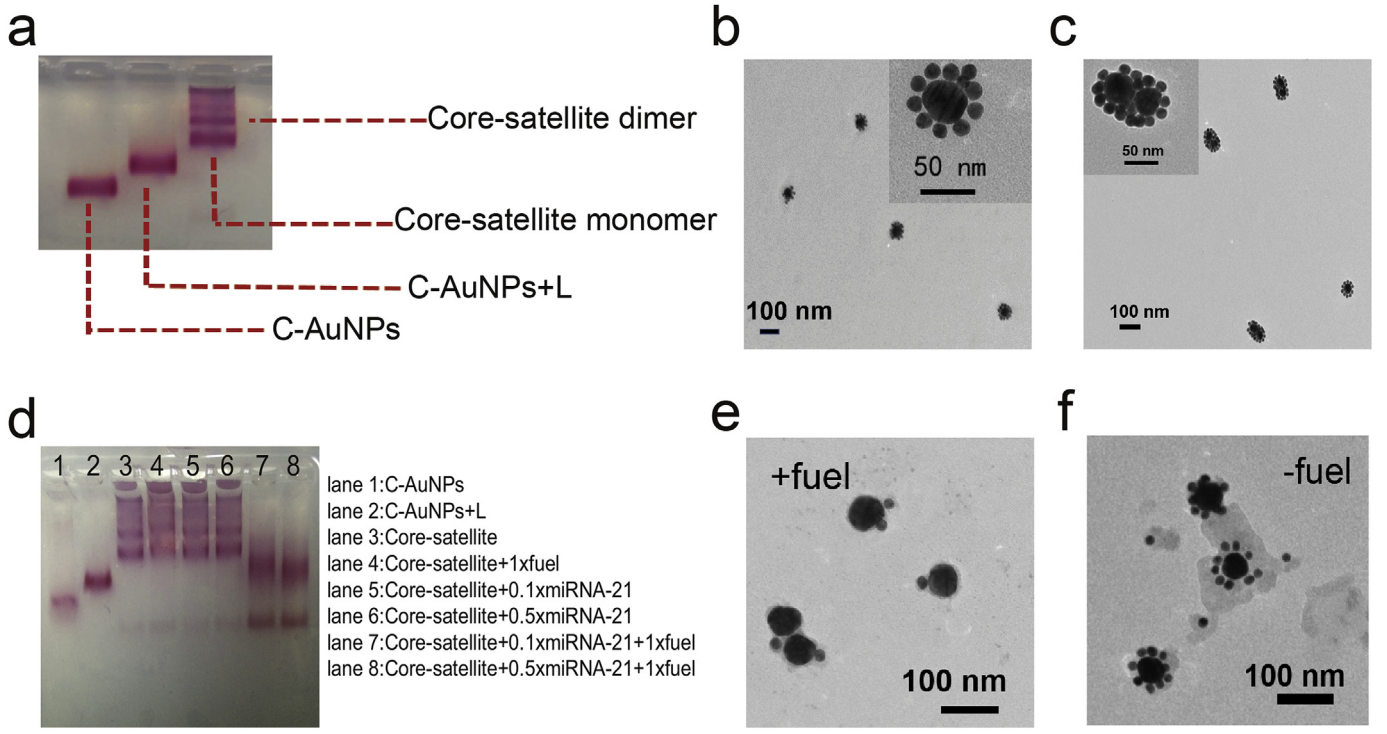

Fig. 2. (a) Agarose gel electrophoresis for C-AuNPs, C-AuNPs + L and core-satellites nanoassembly. (b–c) TEM images of monomer and dimer core-satellites nanostructures. (d) Agarose gel electrophoresis for monitoring the catalytic disassembly reactions. "1 × " represented 1 equivalent of L; "0.1 × " represented 0.1 equivalent of L; "0.5 × " represented 0.5 equivalent of L. (e–f) TEM images of core-satellites for catalytic disassembly reactions in the absence and presence of fuel DNA.

the absence of miRNA-21 catalyst (lane 4) and no changes were observed in lane 5 and lane 6 in the absence of fuel DNA, indicating that miRNA-21 can catalyze the disassembly of core-satellites nanoassembly. Moreover, the TEM images shown in Fig. 2e and f also reveal that the disassembly of core-satellites nanoassembly and SDR had taken place with the presence of target miRNA-21 and fuel. The average particle size of the core-satellites nanoassembly had a negligible change if miRNA-21 was absent (Fig. S8).

MiRNA-141 was used to verify the selectivity of this strategy. Upon the addition of fuel DNA, the DLS of core-satellites nanoassembly containing miRNA-141 changed slightly, whereas the DLS of core-satellites nanoassembly containing miRNA-21 declined greatly (Fig. S9). These findings confirm that the developed strategy is reliable for the detection of miRNA-21. The disassembly kinetics of core-satellites nanoassembly was characterized by DLS (Fig. S10), greater changes of DLS were obtained with prolonger reaction time in the presence of fuel DNA and target miRNA, and the disassembly was almost inactivated after 3 h. To assess the sensitivity of the strategy, target miRNA-21 with different concentrations were analysed. Fig. 3a shows the size distribution curves of DLS obtained at different concentrations of miRNA-21. It can be seen that the size distribution of core-satellites nanoassembly gradually shifted to smaller size regions with the increasing dosage of miRNA-21. As shown in Fig. 3b (inset), a good linear correlation was obtained between the hydrodynamic sizes of particles and the concentration of miRNA-21 within a dynamic range of 5–150 pM. The linear equation was expressed as $y = 11.99 + 0.40x$ with a correlation coefficient of 0.9932, where y is the diameter change of core-satellites nanoassembly measured by DLS, and x is the concentration of target miRNA. The limit of detection (LOD) was calculated to be 0.24 pM as calculated on the basis of the standard deviation of blank values (3σ). The detection performance of the strategy was also compared with that of some reported methods, as shown in Table S2, which further suggested that the developed strategy possesses relatively lower detection limit toward miRNA detection.

To investigate the feasibility of the proposed strategy for real sample analysis, the endogenous level of miRNA-21 was measured in the total RNA samples extracted from three cancer cell lines with miRNA-21 overexpressed (i.e. HeLa, MCF-7 and MDA-MB-231) and a control cell line with minimal level of miRNA-21 (i.e. HEK-293). The concentration of miRNA-21 in each RNA sample was determined by using the standard curve in Fig. 3b. The copy numbers of miRNA-21 per pg of total RNA in HeLa, MCF-7 and MDA-MB-231 cells were calculated to be 347 ± 33, 780 ± 62, 698 ± 54, respectively (Fig. 3c and d and Table S3). Meanwhile, the copy number of miRNA-21 per pg total RNA in MCF-7 cells measured by the developed strategy was consistent with the previously reported qRT-PCR data (Chan et al., 2010) and also in good agreement with the results of the qRT-PCR kit (Fig. S11). These findings reveal that the developed SDR-DLS strategy can specifically recognize target miRNA in cancer cells, and thus has great potential implications for the clinical diagnosis of cancer patients.

3. Conclusions

In summary, an enzyme-free and homogeneous DLS sensing strategy coupled with SDR for sensitive detection of miRNA has been established. Although the strategy was not suitable for real-time monitoring of miRNA in living cells, the procedure of the proposed strategy was relatively simple and thus can be easily conducted in ordinary laboratories. Despite the protocol simplicity, a high sensitivity was achieved due to the integration of cycling reaction for signal amplification and robust DLS for powerful signal readout. Additionally, this strategy exhibits a low detection limit at picomole level and has been proven to be applicable for miRNA detection in biological samples. Therefore, it is believed that this new DLS-based strategy may find wide applications in clinical miRNA diagnostics.

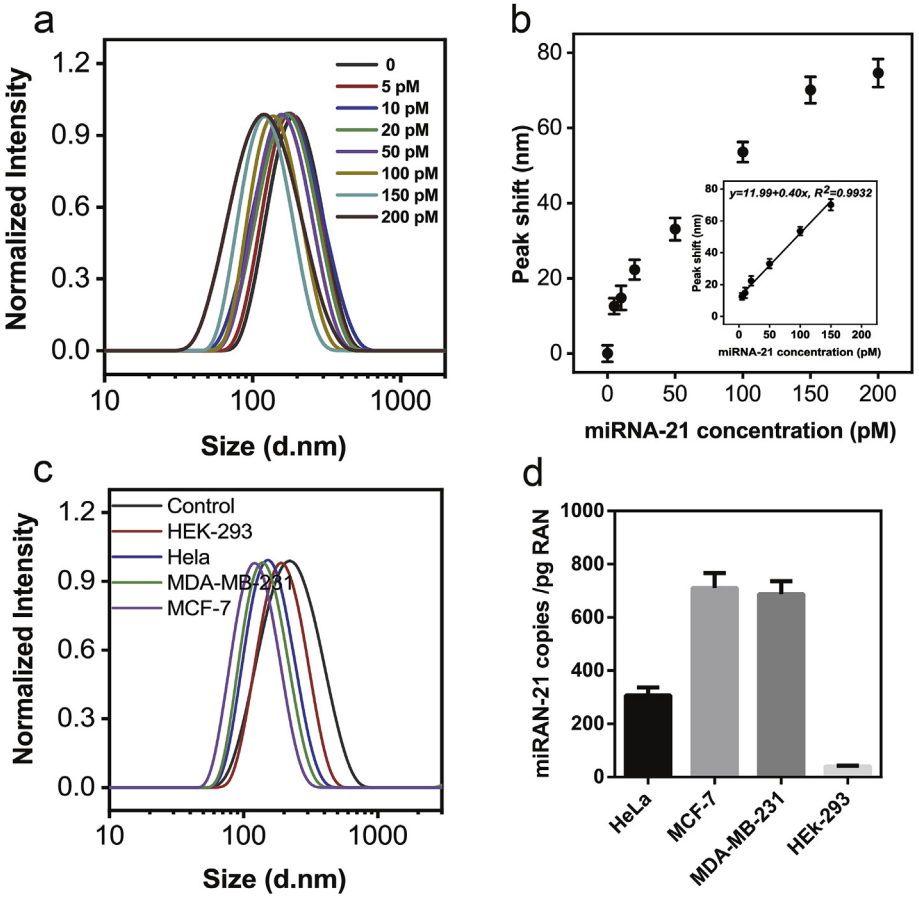

Fig. 3. (a) Distribution curves measured by DLS at different concentrations of miRNA-21. (b) Corresponding relation between the measured average particle size of AuNPs and different concentrations of miRNA-21. (c) DLS measurement of miRNA-21 in the total RNA extracted from four different cell lines. (d) Quantitative analysis of miRNA-21 in the total RNA extracted from four different cell lines.

Declaration of interests

The authors declare that they have no known competing financial interests or personal relationships that could have appeared to influence the work reported in this paper.

CRediT authorship contribution statement

Ganglin Wang: Conceptualization, Methodology, Investigation, Data curation, Writing - original draft, Writing - review & editing. **Mingxia Yu:** Methodology, Funding acquisition, Writing - review & editing. **Guoping Wang:** Supervision, Writing - review & editing, Funding acquisition, Project administration.

Acknowledgments

This work was financially supported by the National Natural Science Foundation of China (No. 61875062, No. 81472033 and No. 30901308), the Fundamental Research Funds for the Central Universities and Hubei Province health and family planning scientific research project (WJ2015Q021).

Appendix A. Supplementary data

Supplementary data to this article can be found online at https://doi.org/10.1016/j.bios.2019.111319.

References

Benes, V., Castoldi, M., 2010. Methods 50, 244–249.
Boon, R.A., Iekushi, K., Lechner, S., Seeger, T., Fischer, A., Heydt, S., Kaluza, D., Treguer, K., Carmona, G., Bonauer, A., Horrevoets, A.J., Didier, N., Girmatsion, Z., Biliczki, P., Ehrlich, J.R., Katus, H.A., Muller, O.J., Potente, M., Zeiher, A.M., Hermeking, H., Dimmeler, S., 2013. Nature 495, 107–110.
Bose, D., Jayaraj, G.G., Kumar, S., Maiti, S., 2013. ACS Chem. Biol. 8, 930–938.
Chan, H.M., Chan, L.S., Wong, R.N.S., Li, H.W., 2010. Anal. Chem. 82, 6911–6918.
Degliangeli, F., Kshirsagar, P., Brunetti, V., Pompa, P.P., Fiammengo, R., 2014. J. Am. Chem. Soc. 136, 2264–2267.
Dong, H., Lei, J., Ding, L., Wen, Y., Ju, H., Zhang, X., 2013. Chem. Rev. 113, 6207–6233.
Dong, H., Meng, X., Dai, W., Cao, Y., Lu, H., Zhou, S., Zhang, X., 2015. Anal. Chem. 87, 4334–4340.
Elghanian, R., Storhoff, J.J., Mucic, R.C., Letsinger, R.L., Mirkin, C.A., 1997. Science 277, 1078–1081.
Guven, B., Dudak, F.C., Boyaci, I.H., Tamer, U., Ozsoz, M., 2014. Analyst 139, 1141–1147.
He, M.Q., Chen, S., Yao, K., Wang, K., Yu, Y.L., Wang, J.H., 2019. Small Methods 1900017.
Jalava, S.E., Urbanucci, A., Latonen, L., Waltering, K.K., Sahu, B., Janne, O.A., Seppala, J., Lahdesmaki, H., Tammela, T.L., Visakorpi, T., 2012. Oncogene 31, 4460–4471.
Jonas, S., Izaurralde, E., 2015. Nat. Rev. Genet. 16, 421–433.
Ladetto, M., Bruggemann, M., Monitillo, L., Ferrero, S., Pepin, F., Drandi, D., Barbero, D., Palumbo, A., Passera, R., Boccadoro, M., Ritgen, M., Gokbuget, N., Zheng, J., Carlton, V., Trautmann, H., Faham, M., Pott, C., 2014. Leukemia 28, 1299–1307.
Lagos, Q.,M., Rauhut, R., Lendeckel, W., Tuschl, T., 2001. Science 294, 853–858.
Lai, C., Liu, X., Qin, L., Zhang, C., Zeng, G., Huang, D., Cheng, M., Xu, P., Yi, H., Huang, D., 2017. Microchim. Acta 184, 2097–2105.
Lai, C., Liu, S., Zhang, C., Zeng, G., Huang, D., Qin, L., Liu, X., Yi, H., Wang, R., Huang, F., Li, B., Hu, T., 2018. ACS Sens. 3, 2566–2573.
Lautner, G., Gyurcsányi, R.E., 2014. Electroanalysis 26, 1224–1235.
Lee, H., Park, J.E., Nam, J.M., 2014. Nat. Commun. 5, 3367.
Lee, J.H., Kim, J.A., Jeong, S., Rhee, W.J., 2016. Biosens. Bioelectron. 86, 202–210.
Li, S., Shang, X., Liu, J., Wang, Y., Guo, Y., You, J., 2017. Anal. Biochem. 528, 47–52.
Li, X., Zhang, H., Tang, Y., Wu, P., Xu, S., Zhang, X., 2017. ACS Sens. 2, 810–816.
Liang, C.P., Ma, P.Q., Liu, H., Guo, X., Yin, B.C., Ye, B.C., 2017. Angew. Chem. Int. Ed. 56, 9077–9081.
Liu, L., Song, C., Zhang, Z., Yang, J., Zhou, L., Zhang, X., Xie, G., 2015. Biosens. Bioelectron. 70, 351–357.
Lu, X., Fan, W., Feng, Q., Qi, Y., Liu, C., Li, Z., 2019. Chem. Eur J. 25, 1701–1705.
Ma, F., Liu, W.J., Zhang, Q., Zhang, C.Y., 2017. Chem. Commun. 53, 10596–10599.
Qin, L., Zeng, G., Lai, C., Huang, D., Xu, P., Zhang, C., Cheng, M., Liu, X., Liu, S., Li, B., Yi, H., 2018. Coord. Chem. Rev. 359, 1–31.
Qin, L., Zeng, G., Lai, C., Huang, D., Zhang, C., Xu, P., Hu, T., Liu, X., Cheng, M., Liu, Y., Hu, L., Zhou, Y., 2017. Sensor. Actuator. B Chem. 243, 946–954.

Shen, W., Deng, H., Ren, Y., Gao, Z., 2013. Chem. Commun. 49, 4959–4961.
Song, C.Y., Yang, Y.J., Yang, B.Y., Sun, Y.Z., Zhao, Y.P., Wang, L.H., 2016. Nanoscale 8, 17365–17373.
Tu, Y., Wu, P., Zhang, H., Cai, C., 2012. Chem. Commun. 48, 10718–10720.
Wang, Q., Yin, B.C., Ye, B.C., 2016. Biosens. Bioelectron. 80, 366–372.
Wu, H., Liu, Y., Wang, H., Wu, J., Zhu, F., Zou, P., 2016. Biosens. Bioelectron. 81, 303–308.
Wu, Z., Liu, G.Q., Yang, X.L., Jiang, J.H., 2015. J. Am. Chem. Soc. 137, 6829–6836.
Xu, W., Xie, X., Li, D., Yang, Z., Li, T., Liu, X., 2012. Small 8, 1846–1850.
Yin, H.S., Li, B.C., Zhou, Y.L., Wang, H.Y., Wang, M.H., Ai, S.Y., 2017. Biosens. Bioelectron. 96, 106–112.
Yu, Y., Chen, Z., Shi, L., Yang, F., Pan, J., Zhang, B., Sun, D., 2014. Anal. Chem. 86, 8200–8205.
Zhong, D., Yang, K., Wang, Y., Yang, X., 2017. Talanta 175, 217–223.